

Entanglement-assisted quantum transduction

Haowei Shi^{1,*} and Quntao Zhuang^{1, 2, †}

¹ *Ming Hsieh Department of Electrical and Computer Engineering,*

University of Southern California, Los Angeles, California 90089, USA

² *Department of Physics and Astronomy, University of Southern California, Los Angeles, California 90089, USA*

A quantum transducer converts an input signal to an output at a different frequency, while maintaining the quantum information with high fidelity. When operating between the microwave and optical frequencies, it is crucial for quantum networking between quantum computers via low-loss optical links, and thereby enabling distributed quantum computing. However, the state-of-the-art quantum transducers suffer from low transduction efficiency due to weak nonlinear coupling, wherein increasing pump power to enhance efficiency leads to inevitable thermal noise from heating. Moreover, we reveal that the efficiency-bandwidth product in such systems is fundamentally limited by pump power and nonlinear coupling coefficient, irrespective of cavity engineering efforts. To resolve the conundrum, we propose to boost the transduction efficiency by consuming entanglement within the same frequency band (e.g., microwave-microwave or optical-optical entanglement). Via a squeezer-coupler-antisqueezer sandwich structure, the protocol enhances the transduction efficiency to unity in the ideal lossless case, given an arbitrarily weak nonlinear coupling, which establishes a high-fidelity quantum communication link without any signal encoding. In practical cavity systems, our entanglement-assisted protocol surpasses the non-assisted fundamental limit of the efficiency-bandwidth product and reduces the threshold cooperativity for positive quantum capacity by a factor proportional to two-mode squeezing gain. Given a fixed cooperativity, our approach increases the broadband quantum capacity by orders of magnitude.

Quantum transduction aims to interconnect quantum computers and quantum processors via converting quantum states between different frequencies [1–3]. It serves as the hinge between the microwave superconducting qubits and the optical telecommunication photons, enabling robust quantum networking [4–7], and ultimately distributed quantum sensing [8] and distributed quantum computing [9, 10]. Despite the proposals based on various physical platforms [11–27], current quantum transduction systems are still far from satisfying, hurdled by a conundrum to balance transduction efficiency, pump-induced heating, and bandwidth [26, 28–32].

An ideal transducer has unity transduction efficiency, quantum-limited noise, and large bandwidth. On the contrary, we show that the efficiency-bandwidth product of traditional quantum transducers are fundamentally limited by the nonlinear coupling coefficient and pump amplitude, regardless of the quality of cavities. Unfortunately, the nonlinear coupling between photons is intrinsically weak, and a stronger pump inevitably induces more thermal noises. Therefore, besides the endeavor from materials science and nanofabrication, paradigm shifts are needed to boost quantum transduction. For example, recent theory works propose discrete-variable [25] or continuous-variable [33] teleportation-based approaches, and Gottesman-Kitaev-Preskill (GKP) encoding [34] for robust transduction even with weak nonlinear coupling. However, the state-of-the-art systems for microwave-optical entanglement generation [32, 35], and optical GKP state engineer-

ing [36] are far from usable. In addition, the latter requires GKP encoding of the input quantum information, not compatible with general quantum networks.

In this work, we propose an entanglement-assisted protocol to achieve a broadband enhancement in transduction efficiency between arbitrary frequencies. As shown in Fig. 1, our protocol only relies on two-mode squeezing between the output port and an ancilla (at the same frequency band) before and after the traditional nonlinear coupler. For example, in optical-to-microwave transduction, it only requires microwave inline squeezing, i.e. parametric amplifier [37–39]. In the absence of loss, for an arbitrarily weak nonlinear coupling, the transduction efficiency can always be enhanced up to unity without any added noise. With broadband cavity electro-optic model taken into account, we show that our protocol goes beyond the efficiency-bandwidth product limit of traditional cavity-enhanced transducers by a factor increasing with the two-mode squeezing gain G . For quantum communication, the broadband one-way quantum capacity is increased by orders of magnitude, lowering the threshold cooperativity for positive quantum capacity by a factor of $\sim 1/G$.

I. PROTOCOL DESIGN

As shown in Fig. 1, a general bosonic transducer converts an input signal S to an output probe P' at different frequency via a nonlinear coupler under a strong pump. The quality of transduction is mainly characterized by an overall photon conversion efficiency η . The transmissivity of the initial probe P is $\kappa \leq 1 - \eta$, as a loss port E is inevitably mixed in with transmissivity (the intrinsic

* hwshi@usc.edu

† qzhuang@usc.edu

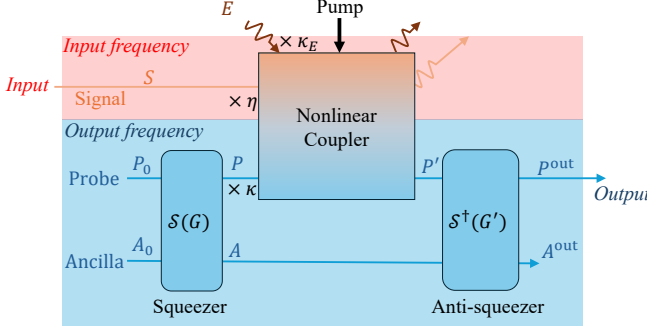


Figure 1. Schematic of the entanglement-assisted transduction protocol. An input signal S is converted to an output probe P^{out} at a different frequency. The protocol is boosted by the entanglement at the output frequency band between the probe P and the ancilla A , which is generated by a two-mode squeezer $\mathcal{S}(G)$ of gain G prior to entering the nonlinear coupler. Then the input signal is converted to the probe frequency via a nonlinear coupler, while an environment E is inevitably mixed in. After the nonlinear coupling, an anti-squeezer $\mathcal{S}^\dagger(G')$ of gain G' amplifies the signal, while the noise background contributed by P_0 and A_0 is nulled to the ground state (vacuum).

loss) $\kappa_E = 1 - \kappa - \eta \geq 0$.

To enhance the performance of quantum transduction, our task is to amplify the signal-carrying probe while keeping the noise background in vacuum state. As shown in Fig. 1, we introduce an additional ancilla system A without alternating the nonlinear coupler. The ancilla and the probe runs a ‘squeezer-coupler-antisqueezer’ protocol with a sandwich structure for the transducer: first the probe and the ancilla are entangled by a two-mode squeezer with gain G ; then, a portion η of the signal S is converted to the probe P' via nonlinear coupling; finally, the converted probe P' and the ancilla A are anti-squeezed with gain G' to produce the final converted output P^{out} . In the absence of the input signal photons, the anti-squeezer is set to null the probe back to vacuum in the low temperature limit. In this work, we ignore the loss in the squeezer and anti-squeezer, as they operate on the probe-ancilla pair at close frequencies (e.g. both in the microwave frequencies [37–39]) thus much easier than the signal-probe coupler.

Below, we elaborate this protocol step by step. Before the signal-probe coupling, we prepare the probe and the ancilla using a two-mode squeezer $\mathcal{S}(G)$ of gain G on initial vacuums P_0 and A_0 . The input-output relation can be conveniently expressed via the linear transform of the field operators

$$\begin{aligned}\hat{\mathcal{E}}_P &= \sqrt{G}\hat{\mathcal{E}}_{P_0} + \sqrt{G-1}\hat{\mathcal{E}}_{A_0}^\dagger, \\ \hat{\mathcal{E}}_A &= \sqrt{G-1}\hat{\mathcal{E}}_{P_0}^\dagger + \sqrt{G}\hat{\mathcal{E}}_{A_0}.\end{aligned}\quad (1)$$

Here $\hat{\mathcal{E}}_X(\omega)$ is the traveling-wave field operator of system X at frequency ω relative to its own carrier, satisfying the commutation relation $[\hat{\mathcal{E}}_X(\omega), \hat{\mathcal{E}}_X^\dagger(\omega')] = \delta(\omega - \omega')$. In

this section, we focus on the narrowband limit and omit ω for simplicity, while the broadband case will be discussed later in the full cavity model. Then, the signal is coupled to the probe via the nonlinear coupler. A widely used nonlinear coupler is the red sideband pumped cavity with χ^2 nonlinear medium e.g. lithium niobate [28]. Its input-output relation in Fourier frequency domain is similar to a beamsplitter [16]:

$$\hat{\mathcal{E}}_{P'} = e^{i\theta_P} \sqrt{\kappa} \hat{\mathcal{E}}_P + e^{i\theta_S} \sqrt{\eta} \hat{\mathcal{E}}_S + \sqrt{\kappa_E} \hat{\mathcal{E}}_E, \quad (2)$$

where $\kappa_E = 1 - \kappa - \eta$ is the intrinsic loss and θ_P , θ_S are phase shifts due to the transduction. We will connect such a beamsplitter model to the cavity electro-optic physics later on. Finally, the probe and the ancilla are anti-squeezed using $\mathcal{S}^\dagger(G')$ to output

$$\hat{\mathcal{E}}_{P^{\text{out}}} = e^{-i\theta_P} \sqrt{G'} \hat{\mathcal{E}}_{P'} - \sqrt{G' - 1} \hat{\mathcal{E}}_A^\dagger, \quad (3)$$

where the phase is chosen to cancel the transduction phase shifts θ_P in Eq. (2). Combining the above, we have the input-output relation from signal S to output

$$\begin{aligned}\hat{\mathcal{E}}_{P^{\text{out}}} &= e^{i(\theta_S - \theta_P)} \sqrt{\eta G'} \hat{\mathcal{E}}_S + \\ &\left(\sqrt{(G-1)\kappa G'} - \sqrt{(G'-1)G} \right) \hat{\mathcal{E}}_{A_0}^\dagger + \text{vac},\end{aligned}\quad (4)$$

where vac are the vacuum terms when the system is ideally cooled. To keep the output to vacuum when no signal is input, one needs to annihilate the coefficient in front of $\hat{\mathcal{E}}_{A_0}^\dagger$ in Eq. (4), leading to

$$G' \leftarrow G'^* \equiv \frac{1}{1 - \kappa + \kappa/G}. \quad (5)$$

One can regard the two-mode anti-squeezer $\mathcal{S}^\dagger(G')$ as an amplifier of the probe, while the first input two-mode squeezer $\mathcal{S}(G)$ reduces the amplifier noise from the anti-squeezer. Eq. (5) indicates that to increase the signal amplification G' without increasing the noise, the input squeezer gain G needs to increase accordingly to provide entanglement assistance. Below, our analysis begins with the ideal lossless case where $\kappa_E = 0$ and then proceeds to the lossy case of $\kappa_E > 0$.

II. LOSSLESS COUPLER: UNITY-EFFICIENCY TRANSDUCTION

Now we assume the lossless limit $\kappa_E = 0$ to gain intuition about the protocol design, which is valid at the cavity overcoupling limit (see Full cavity model). In this case, $\kappa = 1 - \eta$ and the optimal gain in Eq. (5) reduces to $G' \leftarrow G'^* \equiv 1/[\eta + (1 - \eta)/G]$, and the output probe is $\hat{\mathcal{E}}_{P^{\text{out}}}^* = \sqrt{1 - \eta_{EA}} \hat{\mathcal{E}}_{P_0} + \sqrt{\eta_{EA}} e^{i(\theta_S - \theta_P)} \hat{\mathcal{E}}_S$. The entanglement-assisted (EA) transduction efficiency

$$\eta_{EA} = \eta \cdot \frac{G}{G\eta + (1 - \eta)}, \quad (6)$$

which approaches unity in the strong squeezing limit,

$$\eta_{\text{EA}} \rightarrow 1, \text{ when } G' \rightarrow 1/\eta \text{ and } G \rightarrow \infty. \quad (7)$$

At this limit, the output probe $\hat{\mathcal{E}}_{P_{\text{out}}}^* = e^{i(\theta_S - \theta_P)} \hat{\mathcal{E}}_S$ is reflectionless in both quadratures. For a finite gain, the EA protocol increases the efficiency to $\eta_{\text{EA}} \simeq G\eta$ by the amplifier gain factor G , when the original transduction efficiency is low ($\eta \ll 1$). Note that here no-cloning [40] is not violated because the other output of the nonlinear coupler is infinitely noisy at the $G \rightarrow \infty$ limit.

To enable quantum communication with one-way quantum capacity $Q_1 > 0$, one needs the overall conversion efficiency above the *zero-quantum-capacity threshold*, $\eta_{\text{EA}} > 1/2$ [41], leading to $\eta > 1/(G+1)$ which is drastically easier to achieve than the non-EA case of $\eta > 1/2$.

All the above efficiency advantages also hold even if the probe and ancilla are initially in thermal states. Indeed, the transduction efficiency increase comes from the reduction of input-output relations, which holds regardless of the initial states.

III. LOSSY COUPLER

Now we consider general case with intrinsic loss $\kappa_E > 0$. With the choice of Eq. (5), the output probe is $\hat{\mathcal{E}}_{P_{\text{out}}}^* = [G(1 - \kappa) + \kappa]^{-1/2} \left(\sqrt{\kappa} \hat{\mathcal{E}}_P + \sqrt{\eta G} e^{i(\theta_S - \theta_P)} \hat{\mathcal{E}}_S + \sqrt{\kappa_E G} e^{-i\theta_P} \hat{\mathcal{E}}_E \right)$. This leads to the EA ground-state transduction efficiency

$$\eta_{\text{EA}} = \eta \frac{G}{G(1 - \kappa) + \kappa}, \quad (8)$$

which in the strong squeezing limit goes to

$$\eta_{\text{EA}} \rightarrow \frac{1}{1 + \kappa_E/\eta}, \text{ when } G' \rightarrow 1/(1 - \kappa) \text{ and } G \rightarrow \infty. \quad (9)$$

The challenging non-EA zero-quantum-capacity threshold $\eta > 1/2$ is relaxed to the EA threshold $\eta > \kappa_E$ now, which is always achievable via overcoupling.

We evaluate the EA advantage in transduction efficiency in Fig. 2. In subplot (a), we fix the intrinsic loss $\kappa_E = 0.01$ and vary the non-EA efficiency η . The entanglement-assisted efficiency overwhelms the non-EA efficiency (blue diagonal line), even with an intermediate-scale, near-term available squeezing gain $G = 10\text{dB}$. In the inset, we observe the entanglement-assisted efficiency η_{EA} surpasses the zero-quantum-capacity threshold $1/2$ at $\eta \gtrsim \kappa_E = 0.01$, given high squeezing of $G = 30\text{dB}$ —as predicted by Eq. (9). In subplot (b), we fix $\eta = 0.01$ and vary κ_E . At high squeezing, the zero-quantum-capacity threshold $\eta_{\text{EA}} = 1/2$ can be achieved for $\kappa_E \lesssim \eta = 0.01$. For the requirement on squeezing level, we observe that $\eta_{\text{EA}} \rightarrow 1/2$ as $\kappa_E \rightarrow 0$ for $G = 20\text{dB}$, which can be predicted by the ideal cavity formula Eq. (6).

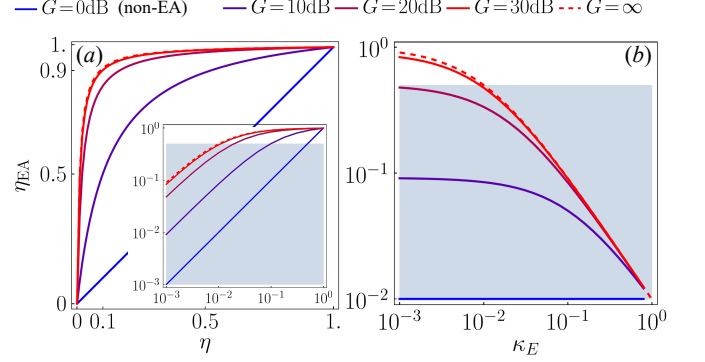


Figure 2. The EA transduction efficiency η_{EA} versus: (a) the non-EA efficiency η , with $\kappa_E = 0.01$; (b) the intrinsic loss κ_E , with $\eta = 0.01$. Inset in (a): Zoom-in near $\eta \rightarrow 0$ in logarithmic scale. Squeezer gain G : from blue to red, G increases from 0dB (non-EA) to 30dB by step of 10dB. Red dashed: $G \rightarrow \infty$ [Eq. (9)]. Blue-shaded region: zero quantum-capacity region $\eta_{\text{EA}} \leq 1/2$. Anti-squeezer gain G' is chosen according to Eq. (5).

IV. FULL CAVITY MODEL

With the basic principle presented in the narrowband regime, now we proceed to introduce the full cavity model for transduction systems. Without loss of generality, we consider the cavity electro-optics system [16, 29, 32], one of the state-of-the-art platforms for quantum transduction. In this case, probe P and signal S are carried on optical/microwave cavity modes, associated with annihilation operators \hat{a}_P, \hat{a}_S satisfying the commutation relation $[\hat{a}_X, \hat{a}_X^\dagger] = 1$, where the subscript $X = P, S$ denotes the probe or signal modes. The quality of the cavities/resonators are characterized by the cavity/resonator external coupling rates and intrinsic loss rates $\gamma_{X,c}$ and $\gamma_{X,0}$. In this paper, we adopt the alternative characterization with the total linewidths $\Gamma_X \equiv \gamma_{X,c} + \gamma_{X,0}$ and the coupling efficiencies $\zeta_X \equiv \gamma_{X,c}/\Gamma_X$. In the interaction picture under the rotating wave approximation, an electro-optics system in the red sideband pumping case can be described by the effective Hamiltonian [16]: $\hat{H}_I = -\hbar g(\hat{a}^* \hat{a}_S^\dagger \hat{a}_P + \alpha \hat{a}_S \hat{a}_P^\dagger)$, where g is the electro-optic nonlinear coupling coefficient in the unit of Hz and α is the in-cavity pump amplitude. The interaction strength is typically characterized by the cooperativity $C = 4|g\alpha|^2/\Gamma_S \Gamma_P$.

Solving the stationary solution of the quantum Langevin equation [16, 42] for \hat{H}_I in the Fourier domain, we obtain the broadband version of Eq. (2). The probe transmissivity spectrum is

$$\sqrt{\kappa(\omega)} e^{i\theta_P(\omega)} = -1 + \frac{2\zeta_P(1 - 2i\frac{\omega}{\Gamma_S})}{(1 - 2i\frac{\omega}{\Gamma_P})(1 - 2i\frac{\omega}{\Gamma_S}) + C}, \quad (10)$$

and the transduction efficiency spectrum is

$$\sqrt{\eta(\omega)}e^{i\theta_S(\omega)} = \frac{2i\sqrt{C}\sqrt{\zeta_P\zeta_S}}{(1-2i\frac{\omega}{\Gamma_P})(1-2i\frac{\omega}{\Gamma_S})+C}. \quad (11)$$

The intrinsic loss spectrum can be obtained correspondingly as $\kappa_E(\omega) = 1 - \kappa(\omega) - \eta(\omega)$. It is worthwhile to note that the cavity/resonator is asymptotically lossless ($\kappa_E(\omega) \rightarrow 0$) at the overcoupling limit ($\zeta_P, \zeta_S \rightarrow 1$). For weak nonlinear coupling $C \ll 1$, the peak conversion efficiency $\eta(\omega = 0) = \zeta_P\zeta_S \cdot 4C/(1+C)^2$; the half-power bandwidth of $\eta(\omega)$ is $B \simeq \min\{\Gamma_S, \Gamma_P\}/2$.

For simplicity, we assume a broadband two-mode squeezing for the squeezer $G(\omega) = G$; for the gain in the anti-squeezing, however, the optimal choice of phase matching $\theta_P(\omega)$ and gain $G''^*(\omega)$ in Eq. (5) will be frequency dependent. Nevertheless, these requirements can be achieved by properly engineering the squeezing cavities. In particular, frequency-dependent squeezing is already being utilized in Laser Interferometer Gravitational-Wave Observatory (LIGO) [43]. The EA transduction efficiency can be obtained from Eq. (8) as $\eta_{\text{EA}}(\omega) = \eta(\omega)G/[G(1-\kappa(\omega)) + \kappa(\omega)]$. At the $G \rightarrow \infty$ limit, we can obtain a simple closed form

$$\eta_{\text{EA}}(\omega)|_{G \rightarrow \infty} = \frac{C\Gamma_S^2\zeta_S}{\Gamma_S^2(C+1-\zeta_P)+4\omega^2(1-\zeta_P)}. \quad (12)$$

Now with entanglement assistance, we observe an improvement in the peak efficiency $\eta_{\text{EA}}(\omega = 0)|_{G \rightarrow \infty} = \zeta_S/[1+(1-\zeta_P)/C]$, and a bandwidth broadening $B_{\text{EA}}|_{G \rightarrow \infty} = \sqrt{1+C/(1-\zeta_P)}\Gamma_S/2$. Remarkably, the EA bandwidth no longer depends on the probe linewidth Γ_P at $G \rightarrow \infty$. Hence the EA advantage is not limited to the weak nonlinear coupling scenarios: even though the on-resonance efficiency can get close to unity with stronger pumping merely, entanglement allows broadband improvement via bandwidth broadening. Similar quantum advantages using non-classical probes have been found in cavity dark matter searches [44, 45].

We plot an example of the EA conversion efficiency spectrum $\eta_{\text{EA}}(\omega)$ in Fig. 3(a). As predicted, we see that the bandwidth of the non-EA case ($G = 0$ dB) is approximately $\Gamma_S/2$, and the EA bandwidth grows as G increases in addition to the peak efficiency advantage. Below, we quantify the EA advantage with three measures of transduction performance: efficiency-bandwidth product, minimum threshold of cooperativity for quantum communication, and broadband quantum capacity.

A. Efficiency-bandwidth product

To quantify the broadband transduction efficiency, we define efficiency-bandwidth product (EBP) as the integration of transduction efficiency over the entire spectrum. This metric is particularly useful in transduction

for broadband quantum sensing applications [45]. Without entanglement assistance, the EBP

$$\mathcal{B} \equiv \int_{-\infty}^{\infty} \eta(\omega)d\omega = \frac{2\pi C\Gamma_P\Gamma_S\zeta_P\zeta_S}{(C+1)(\Gamma_P+\Gamma_S)} \leq \mathcal{B}_{\text{max}} \quad (13)$$

achieves the maximum $\mathcal{B}_{\text{max}} \equiv \pi\zeta_S\zeta_P|g\alpha| \leq \pi|g\alpha|$, at $\Gamma_P = \Gamma_S = 2|g\alpha|$ (i.e. $C = 1$) given a fixed $|g\alpha|$. \mathcal{B}_{max} is a fundamentally limit for the non-EA case determined by the nonlinear coupling coefficient g and pump power $\propto |\alpha|^2$, which cannot be further increased by higher- Q cavity engineering.

Meanwhile, we can also obtain a closed-form solution of EA EBP $\mathcal{B}_{\text{EA}} \equiv \int_{-\infty}^{\infty} \eta_{\text{EA}}(\omega)d\omega$, although too lengthy to be displayed here. Under the same cavity setup $\Gamma_P = \Gamma_S = 2|g\alpha|$, $\zeta_P = \zeta_S = 1$, we obtain $\mathcal{B}_{\text{EA}} = G^{1/4}\pi|g\alpha| \geq G^{1/4}\mathcal{B}_{\text{max}}$, breaking the fundamental limit \mathcal{B}_{max} of the non-EA case. Allowing freely choosing $\Gamma_P = \Gamma_S = 2\sqrt{G}|g\alpha|$, we have $\mathcal{B}_{\text{EA}} \simeq 0.703\sqrt{G}\pi|g\alpha|$ with a \sqrt{G} advantage compared to \mathcal{B}_{max} .

While the above optimal results provide the ultimate limits, here we also consider the practical case of low cooperativity $C \ll 1$. In this case, entanglement can enhance EBP by a factor of G , $\mathcal{B}_{\text{EA}} = G \cdot \mathcal{B}$ when $\zeta_P = \zeta_S = 1$. When $G \rightarrow \infty$, we have a simple closed form expression that applies to any value of C

$$\mathcal{B}_{\text{EA}} \equiv \int_{-\infty}^{\infty} \eta_{\text{EA}}(\omega)d\omega \rightarrow \frac{\pi C\Gamma_S\zeta_S}{2\sqrt{(1+C-\zeta_P)(1-\zeta_P)}}, \quad (14)$$

which diverges as $\zeta_P \rightarrow 1$ as expected.

We plot \mathcal{B}_{EA} in Fig. 3(b) and observe orders of magnitude of EA advantage. Either with Γ_S, Γ_P fixed (solid lines) or with optimized Γ_S, Γ_P over each given $|g\alpha|$ (dot-dashed lines), the EA advantages are demonstrated over the maximal non-EA EBP \mathcal{B}_{max} (blue dot-dashed line) over a wide range of effective nonlinear coupling strength $|g\alpha|$, corresponding to cooperativity $C \in [0.01, 10]$ for the Γ_S, Γ_P fixed cases.

B. Cooperativity threshold

When the electro-optic nonlinear coupling is weak, the maximum transduction efficiency locates at the on-resonance frequency $\omega = 0$. For the non-EA case, we have $\eta(0) = 4C\zeta_P\zeta_S/(1+C)^2$ which surpasses the zero-capacity threshold $1/2$ only when [33]

$$C \geq C_{\text{th}} = -1 + 4\zeta_S\zeta_P - \sqrt{8\zeta_S\zeta_P(2\zeta_S\zeta_P - 1)} \geq 3 - 2\sqrt{2}. \quad (15)$$

With the EA boost, we have the threshold

$$\begin{aligned} C_{\text{th,EA}} = & -1 + \zeta_P((4\zeta_S - 2)G + 2) \\ & - 2\sqrt{\zeta_P G(\zeta_P(4\zeta_S + (1-2\zeta_S)^2G - 1) - 2\zeta_S)}. \end{aligned} \quad (16)$$

When $G \rightarrow \infty$, the threshold converges to $C_{\text{th}} \rightarrow (1 - \zeta_P)/(2\zeta_S - 1)$ when $\zeta_S \geq 1/2$.

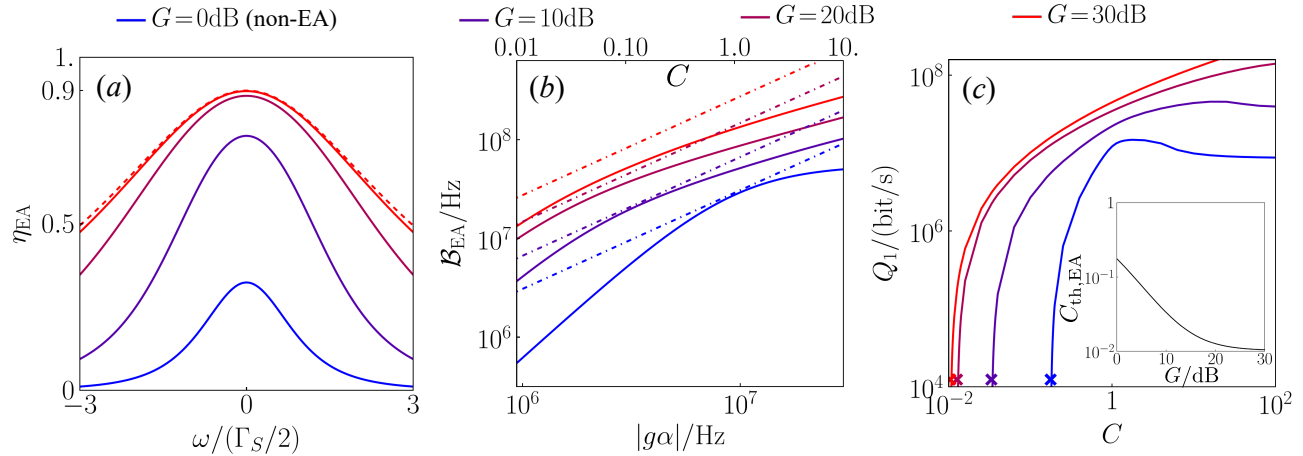


Figure 3. (a) EA transduction efficiency spectrum $\eta_{\text{EA}}(\omega)$ under various squeezing gain G . Cooperativity $C = 0.1$. The dashed line is the $G \rightarrow \infty$ limit obtained from Eq. (12). (b) The EA efficiency-bandwidth product \mathcal{B}_{EA} versus the effective nonlinear coupling strength $|g\alpha|$. The solid lines are under fixed Γ_P, Γ_S , for which we provide the cooperativity C values as the upper axis ticks; while the dot-dashed lines are under optimized Γ_P, Γ_S that maximize \mathcal{B}_{EA} for a given $|g\alpha|$. (c) Broadband quantum capacity rate Q_1 versus cooperativity C under various squeezing gain G . The crosses indicate the zero-quantum-capacity thresholds C_{th} under each G in Eq. (16). Inset: $C_{\text{th},\text{EA}}$ versus G/dB , as given in Eq. (16). The $G = 0\text{dB}$ point goes back to Eq. (15). In all figures, $\zeta_P = \zeta_S = 0.99$; Linewidths $\Gamma_P = 25.8\text{MHz}$, $\Gamma_S = 13.706\text{MHz}$ are chosen according to the high-cooperativity setup in Ref. [29], except the dot-dash lines of (b).

Additional insight can be obtained by considering the overcoupling limit of $\zeta_P = \zeta_S = 1$, threshold in Eq. (16) leads to

$$C_{\text{th},\text{EA}}|_{\zeta_P=\zeta_S=1} = \frac{1}{(\sqrt{G} + \sqrt{1+G})^2} = \frac{1}{4G} + O\left(\frac{1}{G^2}\right), \quad (17)$$

which is lowered by a factor of $1/G$ asymptotically. It is easy to check that $\eta_{\text{EA}}(0)$ approaches unity at the large G limit. We plot the threshold in the inset of Fig. 3(c) for a practical case and identify a reduction by over an order of magnitude when squeezing gain G is large.

C. Broadband quantum information rate

While the efficiency-bandwidth product provides an intuitive characterization of the transduction efficiency, the ultimate quantum information transmission rates are characterized by the quantum capacity [46–48] across the entire spectrum. At the low temperature limit, the one-way quantum capacity of transducer is given as [49, 50]

$$Q_1 = \int \frac{d\omega}{2\pi} \max \left[\log_2 \left(\frac{\eta(\omega)}{1 - \eta(\omega)} \right), 0 \right]. \quad (18)$$

We plot Q_1 versus the cooperativity C for different gain G in Fig. 3(c). Merely $G = 10\text{dB}$ squeezing is sufficient to enable orders of magnitude advantage at low cooperativity. Remarkably, for large C the quantum capacity without probe-ancilla entanglement begins to decay with C as the resonator goes into the oscillatory region with Rabi splitting; by contrast, the quantum capacity as

sisted by probe-ancilla entanglement can further increase with $C \gg 1$.

V. DISCUSSIONS

The most challenging part of the proposed EA transduction is a frequency-dependent inline squeezing. In the optical-to-microwave transduction, the required microwave inline squeezing can be readily realized to high gain [37–39]. Alternative to realizing optical inline squeezing for microwave-to-optical transduction, one can also utilize the optical-to-microwave transduction to generate optical-microwave entanglement from optical-optical entanglement [51, 52], then teleportation enables bi-directional transduction [25, 33].

Finally, we address the connection to related works. Compared with the proposal with in-cavity squeezing [53] that boosts a single quadrature transduction, our approach allows transduction of both quadratures and does not require additional pumping at the cavity that can lead to additional heating. Moreover, an explicit protocol that recovers the initial quantum state is absent in Ref. [53]. Compared with the GKP-based protocol in Ref. [34] that requires the input signal to be GKP encoded, our protocol not only relies on less challenging quantum resources of inline squeezing but also does not require encoding and thus can be applied to transduce general bosonic quantum states. While Ref. [34] only considers the perfect cavity of $\kappa_E = 0$, our protocol shows advantage for practical systems.

ACKNOWLEDGMENTS

HS and QZ proposed the protocol in discussion, performed analyses, generated the figures and wrote the manuscript. The project is supported by Office of Naval Research Grant No. N00014-23-1-2296 and National Sci-

ence Foundation Engineering Research Center for Quantum Networks Grant No. 1941583. QZ also acknowledges support from DARPA MeasQUIT HR0011-24-9-036, National Science Foundation OMA-2326746 and National Science Foundation CAREER Award CCF-2240641.

Appendix A: EBP analyses

To solve the EBP, we make use of the integration formula

$$\int_{-\infty}^{\infty} d\omega \frac{1}{C_1 + 4\omega^2 C_2 + 16\omega^4} = \frac{\pi}{\sqrt{2}\sqrt{C_1}\sqrt{C_2 + 2\sqrt{C_1}}}. \quad (\text{A1})$$

Without the EA [see Eq. (11)], we have

$$\eta(\omega) = \frac{4C\Gamma_P^2\Gamma_S^2\zeta_P\zeta_S}{(C+1)^2\Gamma_P^2\Gamma_S^2 + 4\omega^2(-2C\Gamma_P\Gamma_S + \Gamma_P^2 + \Gamma_S^2) + 16\omega^4}. \quad (\text{A2})$$

With EA and optimal G' [see Eq. (8)], we have

$$\eta_{\text{EA}}(\omega) = \frac{4C\Gamma_P^2\Gamma_S^2\zeta_P\zeta_S G}{\Gamma_P^2\Gamma_S^2(4(C+1)\zeta_P(G-1) + (C+1)^2 - 4\zeta_P^2(G-1)) + 4\omega^2(-2C\Gamma_P\Gamma_S + \Gamma_P^2 + \Gamma_S^2(4\zeta_P(\zeta_P - \zeta_P G + G - 1) + 1)) + 16\omega^4}. \quad (\text{A3})$$

At the overcoupling limit of $\zeta_P = \zeta_S = 1$, the above formula simplifies to

$$\eta_{\text{EA}}(0)|_{\zeta_P=\zeta_S=1} = \eta(0) \frac{G}{[1 + 4(G-1)C/(C+1)^2]}. \quad (\text{A4})$$

Now consider cooperativity $C = 4|g\alpha|^2/\Gamma_S\Gamma_P$, we fix the pump power and the interaction constant, and consider EBP as a function of the cavity parameters Γ_S, Γ_P . With Eq. (A1), we have without EA

$$\begin{aligned} \mathcal{B} &\equiv \int_{-\infty}^{\infty} \eta(\omega) d\omega = \frac{2\pi C\Gamma_P\Gamma_S\zeta_P\zeta_S}{C\Gamma_P + C\Gamma_S + \Gamma_P + \Gamma_S} \\ &= 8\pi|g\alpha|\zeta_P\zeta_S \frac{\tilde{\Gamma}_P\tilde{\Gamma}_S}{(\tilde{\Gamma}_P + \tilde{\Gamma}_S)(4 + \tilde{\Gamma}_P\tilde{\Gamma}_S)}, \end{aligned} \quad (\text{A5})$$

where we have defined $\tilde{\Gamma}_X = \Gamma_X/|g\alpha|$.

For the EA formula, we can also obtain lengthy closed-form solution of EA EBP $\mathcal{B}_{\text{EA}} \equiv \int_{-\infty}^{\infty} \eta_{\text{EA}}(\omega) d\omega$ from Eq. (A1), which we will not display here. For $\zeta_P = \zeta_S = 1$, we have a slightly simpler result,

$$\mathcal{B}_{\text{EA}} = \frac{8\pi\tilde{\Gamma}_P\tilde{\Gamma}_SG|g\alpha|}{\sqrt{(\tilde{\Gamma}_P\tilde{\Gamma}_S(\tilde{\Gamma}_P\tilde{\Gamma}_S + 16G - 8) + 16)\left(\tilde{\Gamma}_P^2 + \tilde{\Gamma}_S^2 + 2\sqrt{\tilde{\Gamma}_P\tilde{\Gamma}_S(\tilde{\Gamma}_P\tilde{\Gamma}_S + 16G - 8) + 16} - 8\right)}}. \quad (\text{A6})$$

[1] N. Lauk, N. Sinclair, S. Barzanjeh, J. P. Covey, M. Saffman, M. Spiropulu, and C. Simon, Perspectives on quantum transduction, *Quantum Sci. Techno.* **5**, 020501 (2020).

[2] D. Awschalom, K. K. Berggren, H. Bernien, S. Bhave, L. D. Carr, P. Davids, S. E. Economou, D. Englund, A. Faraon, M. Fejer, *et al.*, Development of quantum interconnects (quics) for next-generation information tech-

nologies, PRX Quantum **2**, 017002 (2021).

[3] X. Han, W. Fu, C.-L. Zou, L. Jiang, and H. X. Tang, Microwave-optical quantum frequency conversion, *Optica* **8**, 1050 (2021).

[4] A. Acín, J. I. Cirac, and M. Lewenstein, Entanglement percolation in quantum networks, *Nat. Phys.* **3**, 256 (2007).

[5] H. J. Kimble, The quantum internet, *Nature* **453**, 1023 (2008).

[6] S. Wehner, D. Elkouss, and R. Hanson, Quantum internet: A vision for the road ahead, *Science* **362** (2018).

[7] W. Kozlowski and S. Wehner, Towards large-scale quantum networks, in *Proceedings of the Sixth Annual ACM International Conference on Nanoscale Computing and Communication* (2019) pp. 1–7.

[8] Z. Zhang and Q. Zhuang, Distributed quantum sensing, *Quantum Sci. Techno.* **6**, 043001 (2021).

[9] C. Monroe, R. Raussendorf, A. Ruthven, K. R. Brown, P. Maunz, L.-M. Duan, and J. Kim, Large-scale modular quantum-computer architecture with atomic memory and photonic interconnects, *Physical Review A* **89**, 022317 (2014).

[10] S. Barz, E. Kashefi, A. Broadbent, J. F. Fitzsimons, A. Zeilinger, and P. Walther, Demonstration of blind quantum computing, *science* **335**, 303 (2012).

[11] R. W. Andrews, R. W. Peterson, T. P. Purdy, K. Cicak, R. W. Simmonds, C. A. Regal, and K. W. Lehnert, Bidirectional and efficient conversion between microwave and optical light, *Nat. Phys.* **10**, 321 (2014).

[12] J. Bochmann, A. Vainsencher, D. D. Awschalom, and A. N. Cleland, Nanomechanical coupling between microwave and optical photons, *Nat. Phys.* **9**, 712 (2013).

[13] A. Vainsencher, K. Satzinger, G. Peairs, and A. Cleland, Bi-directional conversion between microwave and optical frequencies in a piezoelectric optomechanical device, *Appl. Phys. Lett.* **109**, 033107 (2016).

[14] K. C. Balram, M. I. Davanço, J. D. Song, and K. Srinivasan, Coherent coupling between radiofrequency, optical and acoustic waves in piezo-optomechanical circuits, *Nat. Photonics* **10**, 346 (2016).

[15] M. Tsang, Cavity quantum electro-optics, *Phys. Rev. A* **81**, 063837 (2010).

[16] M. Tsang, Cavity quantum electro-optics. ii. input-output relations between traveling optical and microwave fields, *Phys. Rev. A* **84**, 043845 (2011).

[17] L. Fan, C.-L. Zou, R. Cheng, X. Guo, X. Han, Z. Gong, S. Wang, and H. X. Tang, Superconducting cavity electro-optics: a platform for coherent photon conversion between superconducting and photonic circuits, *Sci. Adv.* **4**, eaar4994 (2018).

[18] Y. Xu, A. A. Sayem, L. Fan, S. Wang, R. Cheng, C.-L. Zou, W. Fu, L. Yang, M. Xu, and H. X. Tang, Bidirectional electro-optic conversion reaching 1% efficiency with thin-film lithium niobate, *arXiv:2012.14909* (2020).

[19] W. Jiang, C. J. Sarabalis, Y. D. Dahmani, R. N. Patel, F. M. Mayor, T. P. McKenna, R. Van Laer, and A. H. Safavi-Naeini, Efficient bidirectional piezoelectromechanical transduction between microwave and optical frequency, *Nat. Commun.* **11**, 1 (2020).

[20] J. Verdú, H. Zoubi, C. Koller, J. Majer, H. Ritsch, and J. Schmiedmayer, Strong magnetic coupling of an ultracold gas to a superconducting waveguide cavity, *Phys. Rev. Lett.* **103**, 043603 (2009).

[21] L. A. Williamson, Y.-H. Chen, and J. J. Longdell, Magneto-optic modulator with unit quantum efficiency, *Phys. Rev. Lett.* **113**, 203601 (2014).

[22] L. Shao, M. Yu, S. Maity, N. Sinclair, L. Zheng, C. Chia, A. Shams-Ansari, C. Wang, M. Zhang, K. Lai, *et al.*, Microwave-to-optical conversion using lithium niobate thin-film acoustic resonators, *Optica* **6**, 1498 (2019).

[23] N. Fiaschi, B. Hensen, A. Wallucks, R. Benevides, J. Li, T. P. M. Alegre, and S. Gröblacher, Optomechanical quantum teleportation, *Nat. Photon.* **15**, 817 (2021).

[24] X. Han, W. Fu, C. Zhong, C.-L. Zou, Y. Xu, A. Al Sayem, M. Xu, S. Wang, R. Cheng, L. Jiang, *et al.*, Cavity piezomechanics for superconducting-nanophotonic quantum interface, *Nat. Commun.* **11**, 1 (2020).

[25] C. Zhong, Z. Wang, C. Zou, M. Zhang, X. Han, W. Fu, M. Xu, S. Shankar, M. H. Devoret, H. X. Tang, *et al.*, Proposal for heralded generation and detection of entangled microwave-optical-photon pairs, *Phys. Rev. Lett.* **124**, 010511 (2020).

[26] M. Mirhosseini, A. Sipahigil, M. Kalaei, and O. Painter, Superconducting qubit to optical photon transduction, *Nature* **588**, 599 (2020).

[27] M. Forsch, R. Stockill, A. Wallucks, I. Marinković, C. Gärtner, R. A. Norte, F. van Otten, A. Fiore, K. Srinivasan, and S. Gröblacher, Microwave-to-optics conversion using a mechanical oscillator in its quantum ground state, *Nat. Phys.* **16**, 69 (2020).

[28] J. Holzgrafe, N. Sinclair, D. Zhu, A. Shams-Ansari, M. Colangelo, Y. Hu, M. Zhang, K. K. Berggren, and M. Lončar, Cavity electro-optics in thin-film lithium niobate for efficient microwave-to-optical transduction, *Optica* **7**, 1714 (2020).

[29] R. Sahu, W. Hease, A. Rueda, G. Arnold, L. Qiu, and J. M. Fink, Quantum-enabled operation of a microwave-optical interface, *Nat. Commun.* **13**, 1276 (2022).

[30] B. M. Brubaker, J. M. Kindem, M. D. Urmey, S. Mittal, R. D. Delaney, P. S. Burns, M. R. Vissers, K. W. Lehnert, and C. A. Regal, Optomechanical ground-state cooling in a continuous and efficient electro-optic transducer, *Phys. Rev. X* **12**, 021062 (2022).

[31] L. Qiu, R. Sahu, W. Hease, G. Arnold, and J. M. Fink, Coherent optical control of a superconducting microwave cavity via electro-optical dynamical back-action, *Nat. Commun.* **14**, 3784 (2023).

[32] R. Sahu, L. Qiu, W. Hease, G. Arnold, Y. Minoguchi, P. Rabl, and J. M. Fink, Entangling microwaves with light, *Science* **380**, 718 (2023).

[33] J. Wu, C. Cui, L. Fan, and Q. Zhuang, Deterministic microwave-optical transduction based on quantum teleportation, *Phys. Rev. Appl.* **16**, 064044 (2021).

[34] Z. Wang and L. Jiang, Passive environment-assisted quantum transduction with gkp states, *arXiv:2401.16781* (2024).

[35] S. Meesala, S. Wood, D. Lake, P. Chiappina, C. Zhong, A. D. Beyer, M. D. Shaw, L. Jiang, and O. Painter, Non-classical microwave-optical photon pair generation with a chip-scale transducer, *Nat. Phys.* **1** (2024).

[36] S. Konno, W. Asavanant, F. Hanamura, H. Nagayoshi, K. Fukui, A. Sakaguchi, R. Ide, F. China, M. Yabuno, S. Miki, *et al.*, Logical states for fault-tolerant quantum computation with propagating light, *Science* **383**, 289 (2024).

[37] K. M. Backes, D. A. Palken, S. A. Kenany, B. M. Brubaker, S. Cahn, A. Droster, G. C. Hilton, S. Ghosh, H. Jackson, S. K. Lamoreaux, *et al.*, A quantum en-

hanced search for dark matter axions, *Nature* **590**, 238 (2021).

[38] M. Xu, R. Cheng, Y. Wu, G. Liu, and H. X. Tang, Magnetic field-resilient quantum-limited parametric amplifier, *PRX Quantum* **4**, 010322 (2023).

[39] J. Y. Qiu, A. Grimsmo, K. Peng, B. Kannan, B. Lienhard, Y. Sung, P. Krantz, V. Bolkhovsky, G. Calusine, D. Kim, *et al.*, Broadband squeezed microwaves and amplification with a josephson travelling-wave parametric amplifier, *Nature Physics* **19**, 706 (2023).

[40] W. K. Wootters and W. H. Zurek, A single quantum cannot be cloned, *Nature* **299**, 802 (1982).

[41] M. M. Wolf, D. Pérez-García, and G. Giedke, Quantum capacities of bosonic channels, *Phys. Rev. Lett.* **98**, 130501 (2007).

[42] C. W. Gardiner and M. J. Collett, Input and output in damped quantum systems: Quantum stochastic differential equations and the master equation, *Phys. Rev. A* **31**, 3761 (1985).

[43] L. McCuller, C. Whittle, D. Ganapathy, K. Komori, M. Tse, A. Fernandez-Galiana, L. Barsotti, P. Fritschel, M. MacInnis, F. Matichard, *et al.*, Frequency-dependent squeezing for advanced ligo, *Phys. Rev. Lett.* **124**, 171102 (2020).

[44] M. Malnou, D. Palken, B. Brubaker, L. R. Vale, G. C. Hilton, and K. Lehnert, Squeezed vacuum used to accelerate the search for a weak classical signal, *Phys. Rev. X* **9**, 021023 (2019).

[45] H. Shi and Q. Zhuang, Ultimate precision limit of noise sensing and dark matter search, *npj Quantum Inf.* **9**, 27 (2023).

[46] S. Lloyd, Capacity of the noisy quantum channel, *Phys. Rev. A* **55**, 1613 (1997).

[47] P. W. Shor, The quantum channel capacity and coherent information, in *lecture notes, MSRI Workshop on Quantum Computation* (2002).

[48] I. Devetak, The private classical capacity and quantum capacity of a quantum channel, *IEEE Trans. Inf. Theory* **51**, 44 (2005).

[49] A. S. Holevo and R. F. Werner, Evaluating capacities of bosonic gaussian channels, *Phys. Rev. A* **63**, 032312 (2001).

[50] C.-H. Wang, F. Li, and L. Jiang, Quantum capacities of transducers, *Nat. Commun.* **13**, 6698 (2022).

[51] H. Vahlbruch, M. Mehmet, K. Danzmann, and R. Schnabel, Detection of 15 db squeezed states of light and their application for the absolute calibration of photoelectric quantum efficiency, *Physical review letters* **117**, 110801 (2016).

[52] T. Kashiwazaki, N. Takanashi, T. Yamashima, T. Kazama, K. Enbutsu, R. Kasahara, T. Umeki, and A. Furusawa, Continuous-wave 6-db-squeezed light with 2.5-thz-bandwidth from single-mode ppls waveguide, *APL Photonics* **5** (2020).

[53] C. Zhong, M. Xu, A. Clerk, H. X. Tang, and L. Jiang, Quantum transduction is enhanced by single mode squeezing operators, *Phys. Rev. Research* **4**, L042013 (2022).